PCCP

Influence of Soluble Oligomeric Aluminum on Precipitation in the Al-KOH-H_2O System

Journal:	*Physical Chemistry Chemical Physics*
Manuscript ID	CP-ART-09-2020-004820.R1
Article Type:	Paper
Date Submitted by the Author:	13-Oct-2020
Complete List of Authors:	Dembowski, Mateusz; Pacific Northwest National Laboratory Graham, Trent; Pacific Northwest National Laboratory Reynolds, Jacob; Washington River Protection Solutions LLC Clark, Sue; Pacific Northwest National Laboratory Rosso, Kevin; Pacific Northwest National Laboratory Pearce, Carolyn; Pacific Northwest National Laboratory,

Influence of Soluble Oligomeric Aluminum on Precipitation in the Al-KOH-H_2O System

Mateusz Dembowski[†*], Trent R. Graham[†], Jacob G. Reynolds[‡], Sue B. Clark[†], Kevin M. Rosso[†], and Carolyn I. Pearce[†]

[†]Pacific Northwest National Laboratory, Richland, Washington 99352, USA

[‡]Washington River Protection Solutions, LLC, Richland, Washington 93352, USA

Abstract

The role of oligomeric aluminate species in the precipitation of aluminum (Al) phases such as gibbsite (α-$Al(OH)_3$) from aqueous hydroxide solutions remains unclear and difficult to probe directly, despite its importance for developing accurate predictions of Al solubility in highly alkaline systems. Precipitation in this system entails a transition from predominantly tetrahedrally coordinated aluminate ($Al(OH)_4^-$) species in solution to octahedrally coordinated Al in gibbsite. Here we report a quantitative study of dissolved Al in the Al-KOH-H_2O system using a combination of molecular spectroscopies. We establish a relationship between changes in ^{27}Al NMR chemical shifts and the relative intensity of Raman vibrational bands, indicative of variations in the ensemble speciation of Al in solution, and the formation of unique contact ion pair interactions with the aluminate dimer, $Al_2O(OH)_6^{2-}$. A strong correlation between the extent of Al oligomerization and the amount of solvated Al was demonstrated by systematically varying the KOH:Al molar ratio. The concentration of dissolved oligomeric Al in solution also directly impacted the particle size and morphology of the precipitated gibbsite. High concentrations of dimeric $Al_2O(OH)_6^{2-}$ yielded smaller and more numerous anhedral to subhedral gibbsite particles, while low concentrations yielded fewer and larger euhedral gibbsite platelets. The collective observations suggest a key role for the $Al_2O(OH)_6^{2-}$ dimer in promoting gibbsite precipitation from solution, with the potassium ion-paired dimer catalyzing a more rapid transformation of Al from tetrahedral coordination in solution to octahedral coordination in gibbsite.

Introduction

The identification of pre-nucleation species in concentrated caustic aluminate solutions has been pursued for over a century and remains an important challenge.[1-3] For example, obtaining a more detailed understanding of this system could improve efficiencies in worldwide aluminum (Al) production via the Bayer process, where Al is extracted from bauxite ore into sodium hydroxide solutions and then re-crystallized as gibbsite (α-$Al(OH)_3$). The precipitation of gibbsite from industrial Bayer liquors is the slowest stage in Al refinement, resulting in increased energy consumption and operational costs. Gibbsite seed crystals are added to improve precipitation kinetics but the yield increase is limited. A better understanding of the precipitation mechanism and the nature of the precipitated phase, is essential to improve efficiency. Along with being a key mineral phase in the Bayer process, gibbsite has a variety of applications as an absorbent,[4] fire-retardant,[5] adjuvant in vaccines,[6] and polishing agent.[7] A number of recent studies have focused on the development of synthetic procedures that lead to the formation of gibbsite particles with controlled size and shape.[8, 9] The need to control the aspect ratio, the prominence of certain crystallographic faces, and the overall size of gibbsite particles is driven in part by its use as a precursor material that undergoes pseudomorphic transformation into a variety of alumina phases, such as γ-, δ-, or χ-Al_2O_3 that are widely used in industrial applications.[8]

In caustic aluminate solutions the tetrahedrally coordinated aluminate anion, $Al(OH)_4^-$ and dianion, $Al_2O(OH)_6^{2-}$ are widely accepted as the two principal Al species. Their presence in solution has been confirmed by experimental techniques including X-ray diffraction,[10] ^{27}Al NMR and Raman spectroscopies,[11, 12] and conductivity measurements.[13] An ab initio molecular dynamics study was used to confirm the stability of $Al(OH)_4^-$ and $Al_2O(OH)_6^{2-}$ moieties, and to predict their spectroscopic signatures. These theoretical insights revealed that other oligomeric Al species, such as the dihydroxo bridged dimer, $Al_2(OH)_8^{2-}$, could also be relevant, and that similarities in the Raman spectra for $Al_2(OH)_8^{2-}$ and $Al(OH)_4^-$ complicates the deconvolution of experimentally obtained spectra.[14, 15] Higher order oligomeric species (e.g. hexamers) have been implicated in the transformation of tetrahedral species in solution to octahedrally coordinated Al in gibbsite and the oxyhydroxide boehmite (γ-AlOOH),[16] but their presence in these concentrated alkaline solutions has not been confirmed experimentally. A recent review of Al speciation under alkaline conditions concluded that all experimentally observed spectroscopic signatures could be accounted for with simple mono- or dimeric Al species,[12] although the exact identity of the dimeric species remains unresolved.[11]

While the Al-NaOH-H_2O system is more common in industry, the inability to crystallize solution phase species in the Na^+ system necessitates exploration of $Al(OH)_4^-$ speciation in chemical analogs, such

as the Al-KOH-H_2O system. In the Al-KOH-H_2O system, the potassium aluminate dimer ($K_2Al_2O(OH)_6$), composed of μ-oxo bridged aluminate tetrahedra, forms the solubility limiting phase in concentrated solutions.[17] Under similar conditions in the Al-NaOH-H_2O system, multiple crystalline sodium aluminate hydrates form, such as the unstable tetrahedral monosodium aluminate hydrate, where Al tetrahedra are bridged by 3 oxygens and one hydroxide, or the octahedral nonasodium bis(hexahydroxy aluminate) trihydroxide hexahydrate, where monomeric aluminate octahedra coordinate solely with hydroxide anions.[18] These sodium aluminate hydrates do not reflect the dominant Al species in solution, but the aluminate dimer moiety, present in the $K_2Al_2O(OH)_6$ solids closely resembles the species expected in both Al-NaOH-H_2O and Al-KOH-H_2O solutions. Thus, the Al-KOH-H_2O system is of interest for understanding relationships between aluminate speciation and conditions that lead to gibbsite crystallization.

Here, a systematic spectroscopic interrogation of the Al-KOH-H_2O system was conducted to determine the factors affecting oligomerization of Al in solution, and the subsequent impact on precipitated phase morphology. Solution conditions were targeted to transition from low alkali concentrations (KOH:Al ratio of 1.00) that favor crystallization of gibbsite, to high alkali concentrations (KOH:Al ratio of 1.66) that favor the crystallization of the $K_2Al_2O(OH)_6$ solid.[19] A multimodal approach to solution characterization, consisting of inductively coupled plasma optical emission spectrometry (ICP-OES), Raman spectroscopy, and ^{27}Al nuclear magnetic resonance (NMR) spectroscopy, allowed the abundance of different Al species to be determined. Scanning electron microscopy (SEM) and X-ray diffraction (XRD) were used to examine correlations between Al solution conditions and the nature of the precipitated solid phases.

Experimental

Wet chemical preparation of solutions. Dissolution of Al wire was carried out in 30 mL Teflon bottles at 25°C, and inside of an N_2-filled glovebox, to minimize the uptake of CO_2. Appropriate quantities of KOH (Fisher Scientific, ACS grade) and H_2O (18 MΩ-cm) were measured, mixed, and allowed to cool (**Table 1**). Subsequently, Al wire (Sigma-Aldrich, 99.999%) was introduced to the reaction vessels ca. 100 mg at a time over a period of three days. Complete dissolution of Al wire (7-14 days) resulted in clear, colorless solutions and a white precipitate in all experiments, with the exception of c2, and c3 which formed only solutions. Resulting suspensions were centrifuged at 8000 RPM for 10 min, decanted, and remaining slurries vacuum filtered and washed with ethanol (Fisher Scientific, ACS grade). Decanted liquids were filtered through a polyvinylidene difluoride syringe filters (0.2 μm, Whatman) and an aliquot was immediately diluted in conc. HNO_3 (Fisher Scientific, Optima trace metal grade) for elemental analysis (ICP-OES). Raman and ^{27}Al nuclear magnetic resonance (NMR) measurements were carried out on filtered solutions. No precipitation was observed following the initial filtration or during subsequent measurements. Presence of advantageous CO_3^{2-} in post-reacted systems was evaluated by Raman spectroscopy (**Figure S1-2**). In the system with highest recorded Al concentration (a1) a very weak signal was noted at ca. 1066 cm^{-1} that likely corresponds to CO_3^{2-}. Attempts to integrate and quantify the contribution of the ca. 1066 cm^{-1} signal as a function of the total signal intensity in the 400-1200 cm^{-1} region were unsuccessful due to its low intensity.

Raman spectroscopy. Measurements were conducted on a Horiba LabRam HR spectrometer in the 100-1200 cm^{-1} spectral region using a 633 nm continuous light source and a 40x optical objective mounted on a Nikon Ti-E inverted microscope. Each spectrum consists of an average of ten, 60 second exposure times. The Multipeak Fitting 2 package, implemented in IgorPro 8 software, was used for linear background correction in the 450-850 cm^{-1} region, and peak deconvolution used three Voigt profiles to describe the signals observed at ca. 535, 623, and 700 cm^{-1}.

NMR spectroscopy. Measurements were conducted using a 750 MHz Varian INOVA narrow-bore spectrometer (17.6 T) with 19.5 μs pulse length (π/2 pulse with respect to $Al(H_2O)_6^{3+}$), 56 dB power level attenuation, 0.6 s acquisition time, 2 s relaxation delay, and 64 scans. Chemical shifts (δ) were referenced using a 4 mm Teflon insert, to a 1 M $Al(H_2O)_6^{3+}$ signal (δ = 0 ppm) prepared from dissolution of $AlCl_3 \cdot 6H_2O$ (Sigma-Aldrich). The standard solution was contained in a 5 mm borosilicate NMR tube, and physically separated from the sample in the Teflon insert, allowing accurate and precise determination of ^{27}Al chemical shifts.

Additional characterization. SEM micrographs were collected on carbon coated (ca. 10 nm) samples using Helios NanoLab 600i SEM (FEI, Hillsboro, OR). ICP-OES was used to measure the elemental composition of the solution phases (Table 1), and XRD was used to identify the precipitated phases, with instrumental details provided in **Supporting Information**.

Table 1. *Experimental conditions for dissolution of Al wire in KOH solutions*

Exp.	Al (g)	KOH (g)	H_2O (g)	Al:KOH (mol)	Al_{meas} (mol/L)	XRD Composition $\%Al(OH)_3$	XRD Composition $\%K_2Al_2(OH)_6$
a1	1.000	2.080	4.000	1.000	5.754	76	24
a2	1.000	2.080	5.000	1.000	3.140	68	32
a3	1.000	2.080	6.000	1.000	1.771	100	0
a4	1.000	2.080	7.000	1.000	1.255	98	2
a5	1.000	2.080	8.000	1.000	0.909	100	0
b1	1.000	2.770	4.000	1.332	7.245	0	100
b2	1.000	2.770	5.000	1.332	5.629	74	26
b3	1.000	2.770	6.000	1.332	3.032	100	0
b4	1.000	2.770	7.000	1.332	1.962	100	0
b5	1.000	2.770	8.000	1.332	1.428	100	0
c1	1.000	3.450	4.000	1.659	4.848	0	100
c2	1.000	3.450	5.000	1.659	5.872	N/A*	N/A*
c3	1.000	3.450	6.000	1.659	5.236	N/A*	N/A*
c4	1.000	3.450	7.000	1.659	3.531	100	0
c5	1.000	3.450	8.000	1.659	2.246	100	0

*Experiments c2 and c3 yielded no solid precipitate

Results and Discussion

Solution speciation

Experiments corresponding to different solution conditions (**Table 1**) were allowed to react for 14 days. Subsequently, the solutions were isolated from any precipitated solid phase (i.e. $Al(OH)_3$ and/or $K_2Al_2O(OH)_6$, **Table 1**) using centrifugation and filtration resulting in homogenous solutions used for spectroscopic analysis. Raman spectra obtained from solutions at initial KOH to Al molar ratio of 1.00, 1.33, and 1.66 and varying H_2O content (**Table 1**) are shown in **Figure 1**. Each experimental series (e.g. a1-5) exhibits a trend of decreasing signal intensity as a function of increasing H_2O content (a1→5), with concurrent reduction of the ca. 535 and 700 cm^{-1} signal intensities (peak A and C) relative to that of 623 cm^{-1} (peak B). The band located at ca. 623 cm^{-1} is assigned to the symmetric stretching of the tetrahedrally coordinated aluminate monomer, $Al(OH)_4^-$, while those at ca. 535 and 700 cm^{-1} are assigned to the products of $Al(OH)_4^-$ oligomerization.[11, 15, 20-23] Moolenaar's interpretation that these additional bands in the Raman spectra (at ca. 535 and 700 cm^{-1}) correspond to formation of the oxo-bridged aluminate dimer, $Al_2O(OH)_6^{2-}$ has become widely accepted, with experimental and computational studies corroborating, but not excluding the possible presence of other dimeric, or higher-order species in these solutions.[14, 15, 23, 24]

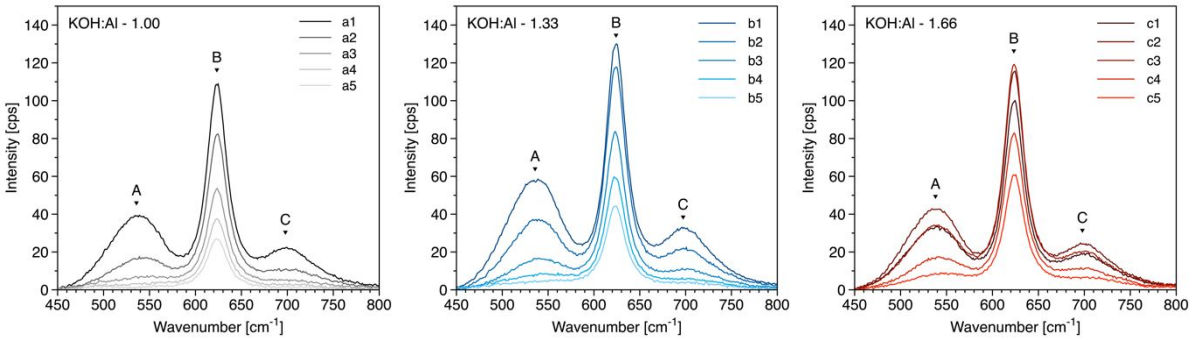

Figure 1. Solution Raman spectra obtained from dissolution of Al wire in KOH at varying initial KOH:Al molar ratios. Peaks at ca. 623 cm^{-1} (B) correspond to $Al(OH)_4^-$ and those at ca. 535 (A), and 700 cm^{-1} (C) to oligomeric Al species.

Raman spectra of the fifteen solutions obtained from dissolution of Al wire in KOH at varying initial KOH:Al molar ratios were deconvoluted and the individual signal contributions were integrated, with the results summarized in **Figure 2**. There is a strong linear correlation (R^2 = 0.9931) between the integrated signal intensity and the concentration of Al in solution, as determined via ICP-OES. However, individual signal contributions do not correlate with Al concentration, especially in the case of the ca. 535, and 700 cm^{-1} signals previously assigned to the products of $Al(OH)_4^-$ oligomerization. In particular, the ratio of the integrated signal intensities associated with oligomeric species (I_{700}/I_{535}) varies between 0.43 and 1.60 (**Figure 3**) with both extremes observed at low to intermediate Al concentrations ($0.91 \leq$ [Al] $mol \cdot L^{-1}$

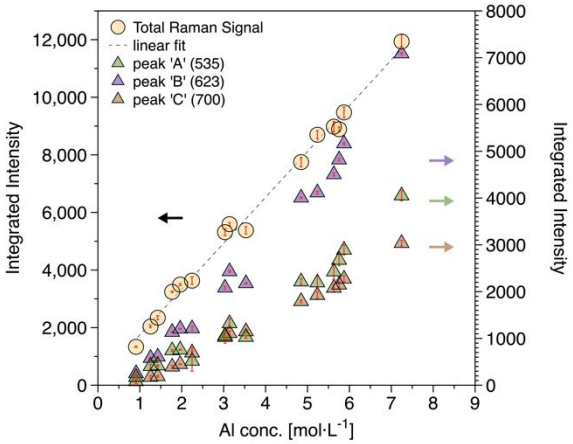

Figure 2. Correlation between the Al concentration in solution (in mol·L^{-1}) and the total and individual integrated Raman signal intensity (left) and the ratio of integrated peak areas of Raman bands associated with formation of higher order Al-oligomers (I_{700}/I_{535}) as a function of increasing Al concentration (right).

solution ≤ 1.96). At intermediate to high Al concentrations (2.25 ≤ [Al] mol·L^{-1} solution ≤ 7.25) the ratio between the two signals shows a steady, system specific (i.e. KOH:Al) decrease. Similar non-linear behavior was credited to the formation of species other than $Al(OH)_4^-$, or $Al_2O(OH)_6^{2-}$, as formation of singular oligomeric species would result in a constant I_{700}/I_{535} ratio.[22, 25] A more recent study suggested that the asymmetric stretch (ca. 725 cm^{-1}), and second harmonic of the asymmetric bending (ca. 650 cm^{-1}) of the $Al(OH)_4^-$ may contribute to the observed intensity of the ca. 700 cm^{-1} band.[20] Numerical analyses performed on current dataset using the relationship $I_{698} = A \times I_{535} + B \times I_{623}$,[20] where A and B are empirical parameters, led to multiple plausible solutions. For example, using $A = 0.50$ and $B = 0.18$ resulted in I_{700}/I_{535} ratio of 0.52±0.02 for samples c1-5. However, applying the same empirical parameters to a1-5 and b1-5 sample sets resulted in the I_{700}/I_{535} ratios of 0.02±0.48 and 0.25±0.36, respectively. Examples of solutions obtained for individual and collective datasets are available in **Supporting Information**. Rather than evaluate different solutions obtained from numerical analysis it was deemed appropriate to perform a sensitivity analysis to evaluate the effect of changes in percent contribution from the second harmonic of the asymmetric bending on the I_{700}/I_{535} ratio. The results spanning a range from zero to 20% contribution presented in **Figure 3A** demonstrate that a single value of B cannot lead to a constant I_{700}/I_{535} ratio. It should be noted, however, that increasing the value of B does lead to convergence of the I_{700}/I_{535} ratio to ca. 0.48 for a subset of the data at higher Al concentrations ([Al] > 3.5 mol·L^{-1}) in accordance with the original study.[20] At lower concentrations ([Al] < 3.5 mol·L^{-1}) increasing contribution from the second harmonic results in divergence of the I_{700}/I_{535} ratio suggesting that in addition to contribution from the

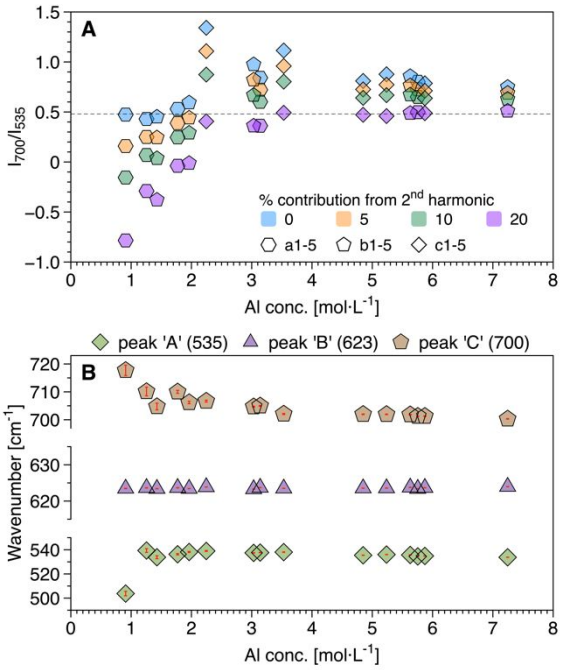

Figure 3. Sensitivity analysis of the I_{700}/I_{535} ratio as a function of contribution from the 2nd harmonic of the asymmetric bend of $Al(OH)_4^-$. Dashed line indicates a ratio of 0.48. Positions of the bands associated with $Al(OH)_4^-$ (peak 'B'), and the products of its oligomerization (peaks 'A' and 'C') as a function of Al concentration.

second harmonic, other factors influence the relative intensities of Raman bands associated with oligomeric Al species

To better understand the unusual and disparate trends in I_{700}/I_{535} values, positions of individual bands were evaluated as a function of Al concentration (**Figure 3B**). Vibrations of the Al-O bonds were previously demonstrated to shift (± 5 cm^{-1}) as a function of interactions of aluminate species (e.g. $Al(OH)_4^-$, $Al_2O(OH)_6^{2-}$) with countercations.[11, 20] The average position and standard deviations for peaks A, B, and C are 534.26±1.86, 623.60±0.19, and 705.05±3.20 cm^{-1}, respectively. Data for the solution at [Al] = 0.91 mol·L^1 was omitted, as the low Al concentration increased the uncertainty in peak position and the standard deviations to ± 8.62, 0.18, and 4.66 cm^{-1} for peak A, B, and C, respectively. Notably, bands associated with products of Al oligomerization (**Figure 2**, peak 'A' and 'C') show shifts that are an order of magnitude higher than that for $Al(OH)_4^-$ (**Figure 2**, peak 'B'). Watling *et al.* reported similar changes, attributing them to variations in speciation that exhibit overlapping resonances at ca. 535 and 700 cm^{-1}.[22, 25] Evaluation of the current data shows no additional bands in the 450-800 cm^{-1} spectral window beyond those indicated in Figure 2 (A-C).

The small standard deviation observed for the signal associated with the aluminate monomer suggests that its interactions with the potassium cation ($Al(OH)_4^-$…K^+) remain relatively consistent across

the experimental series while those between the aluminate dimer and the potassium cation ($Al_2O(OH)_6^{2-}$…K^+), or other products of oligomerization, represented by moving signals at ca. 535 and 700 cm^{-1} change as a function of solution composition (**Figure 3B**). We hypothesize that the observed patterns in peak positions are driven by the population changes between: (i) solvent separated (SSIPs); and (ii) contact ion pairs (CIPs). Due to the high idealized symmetry of $Al(OH)_4^-$ (T_d), its interactions with cations are expected to be non-directional and can be categorized as mono- or bidentate in case of CIPs. Higher order oligomers, such as $Al_2O(OH)_6^{2-}$, have significantly lower symmetry (C_{2v} or lower) and can engage in a number of unique CIPs. For example, $Al_2O(OH)_6^{2-}$ can form CIPs via the terminal -$Al(OH)_3$ groups, or the bridging Al-O-Al motif (**Figure S3**). Consequently, the shifts observed in the Raman bands associated with higher order oligomers can be explained by an ensemble shift between SSIP and CIP or two unique types of CIPs. This interpretation is consistent with the conclusions of previous work that spectroscopic features of concentrated aluminate solutions can be accounted for by ensembles of mono- and dimeric Al species as well as their ion pairs.[20]

For a quantitative understanding of the effect of H_2O and OH^- on Al solubility and subsequent aluminate oligomerization in the KOH-Al-H_2O system, it was assumed that the area under the peak at 623 cm^{-1} was proportional to the concentration of $Al(OH)_4^-$. Subsequently, the extent of oligomerization was calculated by determining the area under the peaks at ca. 535 and 700 cm^{-1} as a function of total integrated Raman intensity in the 450-850 cm^{-1} region and assuming constant and identical molar scattering coefficients for all species in accordance with previously reported methodology.[20] **Figure 4** summarizes the relationship between different reaction conditions, the concentration of Al in solution, and the extent of oligomerization. Overall, decreasing water content (increasing Al, and KOH concentration) at constant Al to KOH ratio (e.g. a5 → a1) results in higher concentration of Al in solution and a higher degree of oligomerization. Notably, the identity of the solubility limiting phase does not

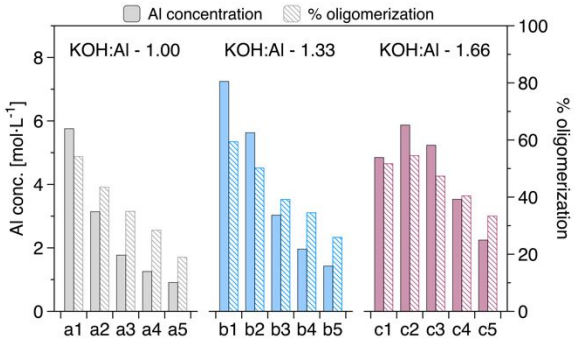

Figure 4. Correlation between the Al concentration in solution and the extent of oligomerization as a function of test conditions.

appear to have a significant effect on the species present in solution. For example, the experimental series a1-5 transitions from a mixed gibbsite/$K_2Al_2O(OH)_6$ solid phase (a1) to pure gibbsite (a5) (**Figure S4-8**), while the relative degree of oligomerization shows a steady, concentration-dependent decrease.

Although the degree of oligomerization is highest in the $K_2Al_2O(OH)_6$ solubility limiting regime (59.38%, b1, **Figure S9**), gibbsite-controlled systems show up to 40.44% (c4, **Figure S15**) of Al species associated with higher-order Al species, indicating that they might play a role in the transformation between four-coordinate solution species, and six-coordinate solid phases such as gibbsite or boehmite. There is also a strong correlation between the [Al] in solution, and the proportion of the total Raman signal assigned to oligomeric species (**Figure 4**). Specifically, increasing the extent of oligomerization from ca. 19% (a5) to 54% (a1) results in a nearly six fold increase in dissolved [Al] present in solution. This observation is consistent with prior hypotheses linking unusually high levels of dissolved Al in caustic solutions to the formation of higher order Al species.[11, 26, 27] However, at higher [OH], as in the experiments with OH:Al of 1.66, the trend between increasing [Al] and the extent of oligomerization breaks down (c2 $\rightarrow$ c3, **Figure 4**) due to the decrease in solubility of $K_2Al_2O(OH)_6$ at higher [OH].[28]

^{27}Al NMR spectra were collected using a high-field instrument (17.6 T) and a physically separated standard to accurately determine the chemical shifts (δ) for the same solutions that were evaluated by Raman spectroscopy. The spectra are characterized by a single resonance at ca. 80 ppm showing a strong linear correlation (R^2 = 0.9868) between their integrated signal intensity and [Al] in solution (**Figure S17**). A similar correlation was observed when the integrated signal intensity was normalized against that of the internal standard (**Figure S18**). The decrease in R^2 for the ^{27}Al NMR data, compared to Raman data, is likely due to the background signal of the NMR probe and broad signals (34.1 ≤ FWHM(Hz) ≤ 944.2)

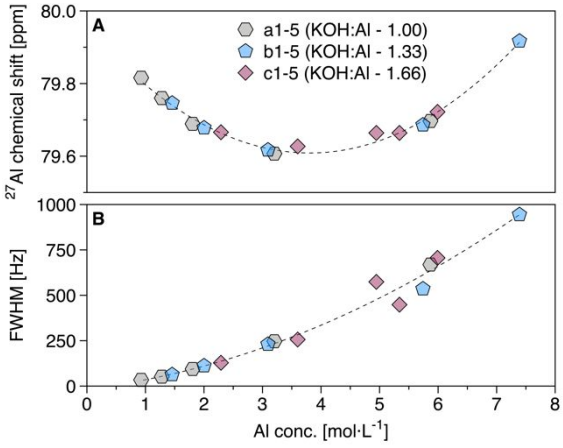

Figure 5. (A) ^{27}Al NMR chemical shift and (B) full width at half max (FWHM) of the ^{27}Al signal as a function of Al concentration.

increasing uncertainty in peak integration. Quantitatively the linear relationship between Al concentration and intensity indicates that either no 'NMR-invisible' Al species are formed, or that they form at a constant rate independent of changing reaction conditions with the observed chemical shift indicating Al in the tetrahedral form.[29-32] **Figure 5** summarizes ^{27}Al chemical shifts and FWHM as a function of [Al] in solution.

Each set of experimental conditions (e.g. a1-5) shows a pseudo-parabolic trend for chemical shifts as a function of [Al] (**Figure 5a**), and a concurrent non-linear increase of FWHM with increasing [Al]. These changes can be attributed to a combination of: (i) variable ensemble of Al species; (ii) ion-ion interactions; and (iii) increasing viscosity. The presence of a single ^{27}Al resonance in all spectra indicates rapid interconversion between the monomeric $Al(OH)_4^-$ and the products of its oligomerization (e.g. $Al_2O(OH)_6^{2-}$). Subtle but systematic changes in the chemical shift are a result of changes in the population-weighted average of the chemical shifts corresponding to the different species (e.g. $Al(OH)_4^-$, $Al_2O(OH)_6^{2-}$, and their ion pairs) identified using Raman spectroscopy (**Figure 4**). Increasing FWHM with increasing [Al] occurs due to the increasing solution viscosity with possible contributions from dynamic exchange of Al species. dynamic equilibrium between different Al species present in solution, and increasing solution viscosity.

Using the relative abundance of mono- and oligomeric Al species determined by Raman spectroscopy the upfield shift of ^{27}Al resonances observed at low-to-intermediate [Al] ($0.65 \leq$ [Al] mol·kg^{-1} solution ≤ 2.50) was attributed to increasing abundance of higher order species that have a lower chemical shift than monomeric aluminate. This interpretation is qualitatively consistent with polymerized Al tetrahedra present in Al_{13} Keggin structures[33-36] and zeolites[37, 38] at chemical shifts of ca. 60-70 ppm, and the trends observed in a recent study comparing chemical shifts of solid-state $Al(OH)_4^-$ and $Al_2O(OH)_6^{2-}$ species.[39] At intermediate-to-high [Al] ($3.53 \leq$ [Al] mol·L^{-1} ≤ 7.25) the downfield chemical shift is attributed to an increase in ion pairing. Specifically, results presented in **Figure 3** indicate that although the position of the central band ($Al(OH)_4^-$, B) remains constant across all [Al], that of the signatures associated with products of Al oligomerization (A and C, $Al_2O(OH)_6^{2-}$) show consistent shifts from 539.38 and 710.13 cm^{-1} at 1.26 mol·L^{-1} to 533.78 and 700.30 cm^{-1} at 7.25 mol·L^{-1}. These shifts indicate formation of strong contact ion pairs between $Al_2O(OH)_6^{2-}$ (and other products of oligomerization) and K^+ at high [Al].[20] Analogous trends in ^{27}Al chemical shifts were reported in a prior study.[12]

Collectively, the trend across the experimental series (e.g. a5 $\rightarrow$ 1) is consistent with formation of the tetrahedrally coordinated, oxo-bridged aluminate dimer, $Al_2O(OH)_6^{2-}$ according to **equation 1**:

$$2Al(OH)_4^- \rightleftharpoons Al_2O(OH)_6^{2-} + H_2O \qquad \text{Eq. 1}$$

Formation of other oligomeric species such as $Al_2(OH)_8^{2-}$, which has been proposed on the basis of ab initio molecular dynamics calculations,[14, 15] might also take place according to **equation 2**:

$$2Al(OH)_4^- \rightleftharpoons Al_2(OH)_8^{2-} \quad \text{Eq. 2}$$

but since its equilibrium expression does not involve H_2O, formation of $Al_2(OH)_8^{2-}$ would be favored under different chemical conditions than that of $Al_2O(OH)_6^{2-}$. In addition, the single ^{27}Al NMR resonance in all spectra, attributed to four-coordinate Al species, does not support the formation of five-coordinate Al containing $Al_2(OH)_8^{2-}$ dimer. This is consistent with prior studies suggesting that formation of five-coordinated Al only takes place under biochemically and geologically relevant conditions ($4.3 < pH < 7$).[29] Five coordinated Al has also been measured in solid materials after vacuum drying or under dry reaction conditions.[40] It should be noted that quantification of ^{27}Al NMR is extremely challenging due to the quadrupolar nature of the nucleus. As such, linear relationship between the concentration of Al and the signal intensity does not conclusively rule out the presence of other five- or six-coordinate species that might be characterized by low local symmetry or rapid interchange. [11, 16, 41] Nonetheless, the wide range of conditions explored in this study paired with dynamic changes in the relative concentration of $Al(OH)_4^-$ and $Al_2O(OH)_6^{2-}$ make it unlikely that a third, 'NMR-invisible' Al species would be present at constant abundance in all evaluated solutions.

Thus, the combination of Raman and ^{27}Al NMR reveal formation of higher-order Al species with signatures that are consistent with a single species, the aluminate dimer $Al_2O(OH)_6^{2-}$. Prior spectroscopic irregularities observed in Raman spectra can be accounted for with the multi-modal nature of ion pairing that occurs between the $Al_2O(OH)_6^{2-}$ and one, or more, cation. The presence of tetrahedrally coordinated oligomers, Al_n ($n<2$) is also not supported, due to persistence of three Raman bands observed across all experimental conditions and the high degree of correlation between the concentration of Al in solution and integrated band intensity.

Effect of experimental conditions on particle morphology

PXRD analysis of solids after the different experiments indicated formation of gibbsite, and/or $K_2Al_2O(OH)_6$ as the only solubility limiting phases (**Table 1**, **Figure S4-16**) in the Al-KOH-H_2O system, in accordance with prior studies.[28] SEM analysis of the pure $K_2Al_2O(OH)_6$ phase obtained from experiment c1 (**Figure S19**) reveals euhedral equant particles ranging from ca. 5 to 30 μm in size. Micrographs of gibbsite particles obtained from experiments with KOH:Al of 1.00 are shown in **Figure 6**.

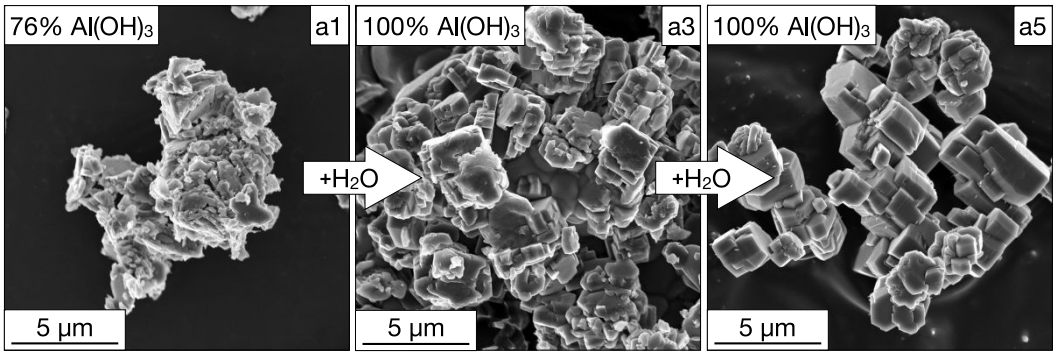

Figure 6. SEM micrographs of gibbsite particles formed in experiments characterized by KOH:Al of 1.00.

The gibbsite particles observed across the experimental series (a1→5) show a trend of increasing particle size, along with decreasing aspect ratio of basal (0 0 1) to prismatic (1 0 0) and (1 1 0) faces, transitioning from anhedral to subhedral platelets (**Figure 6**, left) to euhedral pseudo-hexagonal prisms with significant amount of particles intergrowths and edge-to-edge agglomeration (**Figure 6**, right).[42] These changes in particle size and shape, in combination with Raman data, reveal an inverse correlation between the concentration of higher-order Al species ($Al_2O(OH)_6^{2-}$) in solution, and increasing size and euhedral nature of the resulting gibbsite particles. The SEM results suggest that high concentrations of $Al_2O(OH)_6^{2-}$ in solution promote nucleation of gibbsite, but impede growth of precipitated gibbsite particles, presumably by sorption to, and passivation of, the (0 0 1) face. Studies evaluating the morphology of gibbsite particles precipitated from both synthetic[42-44] and industrial[1, 45] Bayer liquors characterized by lower fraction of oligomerized Al in solution noted similar trends of increased size and decreasing aspect ratio of (0 0 1) to (1 0 0) and (1 1 0) faces. The effect of additional species present in concentrated aluminate solutions on the morphology of resulting gibbsite particles is complex,[46] with some studies suggesting the presence of small amounts of inorganic contaminants has subtle impact,[42] while others indicating otherwise in the case of oxalic acid.[47] Further studies are necessary to establish the relationship between the presence of elevated concentrations of oligomeric aluminate species and the morphology of the precipitated gibbsite particles.[48]

Conclusions

This quantitative interrogation of the Al-KOH-H_2O system was conducted to reduce uncertainties associated with the speciation of Al in solution prior to precipitation of gibbsite, and the mechanism of transformation from four- to six-coordinate Al during precipitation. Systematic variations of the KOH:Al ratio, with subsequent elemental analysis and Raman spectroscopy revealed changes in the ensemble of Al species. Higher alkali concentrations led to formation of tetrahedrally coordinated aluminate dimers,

$Al_2O(OH)_6^{2-}$ at the expense of aluminate monomers, $Al(OH)_4^-$. Variations in the integrated intensity of the Raman bands associated with $Al_2O(OH)_6^{2-}$ arise due to formation of unique contact ion pairs involving the terminal -$Al(OH)_3$, or bridging Al-O-Al motifs, in addition to the previously described contribution from the second harmonic. The relative abundance of $Al(OH)_4^-$, $Al_2O(OH)_6^{2-}$, and their ion pairing behavior, determined via Raman spectroscopy, were subsequently used to interpret trends observed in ^{27}Al NMR spectroscopy data. The upfield shift of the ^{27}Al resonances at intermediate Al concentrations was attributed to change in the ensemble of Al species towards $Al_2O(OH)_6^{2-}$, while the downfield shift at high Al concentrations was attributed to formation of strong $Al_2O(OH)_6^{2-}$…K^+ contact ion pairs. Collectively, changes in solution Raman and ^{27}Al NMR spectroscopy are consistent with presence of two species, $Al(OH)_4^-$ and $Al_2O(OH)_6^{2-}$ and their ion pairs. Analysis of the phase morphology by XRD and SEM respectively, of the solubility-limiting phases formed under different experimental conditions revealed an inverse correlation between the abundance of $Al_2O(OH)_6^{2-}$ in solution, and the size of resulting gibbsite particles. The $Al_2O(OH)_6^{2-}$ species is thus hypothesized to play an important role in the transformation from four- to six-coordinate Al species (gibbsite), while simultaneously passivating the surfaces of the resulting particles.

Acknowledgements

This research was supported as part of IDREAM (Interfacial Dynamics in Radioactive Environments and Materials), an Energy Frontier Research Center funded by the U.S. Department of Energy (DOE) Office of Science, Basic Energy Sciences (BES). Raman and NMR spectroscopy, XRD and SEM data were collected using the William R. Wiley Environmental Molecular Sciences Laboratory (EMSL, grid.436923.9), a national scientific user facility sponsored by the DOE's Office of Biological and Environmental Research located at Pacific Northwest National Laboratory (PNNL) under proposal number 49771. PNNL is a multiprogram national laboratory operated for DOE by Battelle Memorial Institute under Contract No. DE-AC05-76RL0-1830.

Author Information

*current affiliation – Los Alamos National Laboratory, Los Alamos, NM 87545

References

(1) Freij, S. J.; Parkinson, G. M., Surface Morphology and Crystal Growth Mechanism of Gibbsite in Industrial Bayer Liquors. *Hydrometallurgy* **2005,** *78*, 246-255.

(2) Freij, S. J.; Parkinson, G. M.; Reyhani, M. M., Atomic Force Microscopy Study of the Growth Mechanism of Gibbsite Crystals. *Phys. Chem. Chem. Phys.* **2004,** *6*, 1049-1055.

(3) Lee, S. S.; Schmidt, M.; Sturchio, N. C.; Nagy, K. L.; Fenter, P., Effect of pH on the Formation of Gibbsite-Layer Films at the Muscovite (001) Water Interface. *J. Phys. Chem. C* **2019,** *123*, 6560-6571.

(4) Huittinen, N.; Rabung, T.; Lutzenkirchen, J.; Mitchell, S. C.; Bickmore, B. R.; Lehto, J.; Geckeis, H., Sorption of Cm(III) and Gd(III) onto Gibbsite, alpha-$Al(OH)_3$: A Batch and TRLFS Study. *J. Colloid. Interf. Sci.* **2009,** *332*, 158-164.

(5) Yen, Y. Y.; Wang, H. T.; Guo, W. J., Synergistic Effect of Aluminum Hydroxide and Nanoclay on Flame Retardancy and Mechanical Properties of EPDM Composites. *J. Appl. Polym. Sci.* **2013,** *130*, 2042-2048.

(6) Ulanova, M.; Tarkowski, A.; Hahn-Zoric, M.; Hanson, L. A., The Common Vaccine Adjuvant Aluminum Hydroxide Up-Regulates Accessory Properties of Human Monocytes via an Interleukin-4 Dependent Mechanism. *Infect. Immun.* **2001,** *69*, 1151-1159.

(7) Mori, S.; Nakajima, T., Toothpaste Composition. Google Patents: 2000.

(8) Zhang, X.; Huestis, P. L.; Pearce, C. I.; Hu, J. Z.; Page, K.; Anovitz, L. M.; Aleksandrov, A. B.; Prange, M. P.; Kerisit, S.; Bowden, M. E.; Cui, W.; Wang, Z.; Jaegers, N. R.; Graham, T. R.; Dembowski, M.; Wang, H.-W.; Liu, J.; N'Diaye, A. T.; Bleuel, M.; Mildner, D. F. R.; Orlando, T. M.; Kimmel, G. A.; La Verne, J. A.; Clark, S. B.; Rosso, K. M., Boehmite and Gibbsite Nanoplates for the Synthesis of Advanced Alumina Products. *ACS Appl. Nano Mater.* **2018,** *1*, 7115-7128.

(9) Zhang, X.; Zhang, X. W.; Graham, T. R.; Pearce, C. I.; Mehdi, B. L.; N'Diaye, A. T.; Kerisit, S.; Browning, N. D.; Clark, S. B.; Rosso, K. M., Fast Synthesis of Gibbsite Nanoplates and Process Optimization using Box-Behnken Experimental Design. *Cryst. Growth. Des.* **2017,** *17*, 6801-6808.

(10) Radnai, T.; May, P. M.; Hefter, G. T.; Sipos, P., Structure of Aqueous Sodium Aluminate Solutions: A Solution X-ray Diffraction Study. *J. Phys. Chem. A* **1998,** *102*, 7841-7850.

(11) Sipos, P., The Structure of Al(III) in Strongly Alkaline Aluminate Solutions - A Review. *J. Mol. Liq.* **2009,** *146*, 1-14.

(12) Sipos, P.; Hefter, G.; May, P. M., Al-27 NMR and Raman Spectroscopic Studies of Alkaline Aluminate Solutions with Extremely High Caustic Content - Does the Octahedral Species $Al(OH)_6^{3-}$ Exist in Solution? *Talanta* **2006,** *70*, 761-765.

(13) Barcza, L.; Palfalvirozsahegyi, M., The Aluminate Lye as a System of Equilibria. *Mater. Chem. Phys.* **1989,** *21*, 345-356.

(14) Gale, J. D.; Rohl, A. L.; Watling, H. R.; Parkinson, G. M., Theoretical Investigation of the Nature of Aluminum-Containing Species Present in Alkaline Solution. *J. Phys. Chem. B* **1998,** *102*, 10372-10382.

(15) Pouvreau, M.; Dembowski, M.; Clark, S. B.; Reynolds, J. G.; Rosso, K. M.; Schenter, G. K.; Pearce, C. I.; Clark, A. E., Ab Initio Molecular Dynamics Reveal Spectroscopic Siblings and Ion Pairing as New Challenges for Elucidating Prenucleation Aluminum Speciation. *J. Phys. Chem. B* **2018,** *122*, 7394-7402.

(16) Buvári-Barcza, Á.; Rózsahegyi, M.; Barcza, L., Hydrogen Bonded Associates in the Bayer Process (In Concentrated Aluminate Lyes): The Mechanism of Gibbsite Nucleation. *J. Mater. Chem.* **1998**, *8*, 451-455

(17) Johansson, G.; Hope, H.; Nevald, R.; Frank, V.; Brunvoll, J.; Bunnenberg, E.; Djerassi, C.; Records, R. Crystal Structure of the Potassium Aluminate $K_2[Al_2O(OH)_6]$. Acta Chem. Scand. **1966**, 20, 505−515.

(18) Graham, T. R.; Gorniak, R.; Dembowski, M.; Zhang, X.; Clark, S. B.; Pearce, C. I.; Clark, A. E.; Rosso, K. M., Solid-State Recrystallization Pathways of Sodium Aluminate Hydroxy Hydrates. *Inorg. Chem.* **2020**, *59*, 6857-6865

(19) Luo, M.; Ye, J.; Xue, J.; Liu, C.; Song, X.; Yu, J. Phase Equilibrium in the Ternary System K_2O–Al_2O_3–H_2O at 323.15, 333.15, 343.15, and 353.15 K**.** *J. Chem. Eng.* **2020**, *65*, 3463-3471

(20) Sipos, P.; May, P. M.; Hefter, G., Quantitative Determination of an Aluminate Dimer in Concentrated Alkaline Aluminate Solutions by Raman Spectroscopy. *Dalton Trans.* **2006,** *2*, 368-375.

(21) Johnston, C. T.; Agnew, S. F.; Schoonover, J. R.; Kennedy, J. W.; Page, B.; Osborn, J.; Corbin, R., Raman Study of Aluminum Speciation in Simulated Alkaline Nuclear Waste. *Environ. Sci. Technol.* **2002,** *36*, 2451-2458.

(22) Watling, H., Spectroscopy of Concentrated Sodium Aluminate Solutions. *Appl. Spectrosc.* **1998,** *52*, 250-258.

(23) Moolenaar, R. J.; Evans, J. C.; Mckeever, L. D., Structure of Aluminate Ion in Solutions at High pH. *J. Phys. Chem.* **1970,** *74*, 3629-3636.

(24) Bogatko, S.; Geerlings, P., Factors Influencing Al^{3+}-Dimer Speciation and Stability from Density Functional Theory Calculations. *Phys. Chem. Chem. Phys.* **2012,** *14*, 8058-8066.

(25) Watling, H. R.; Fleming, S. D.; van Bronswijk, W.; Rohl, A. L., Ionic Structure in Caustic Aluminate Solutions and the Precipitation of Gibbsite. *J. Chem. Soc., Dalton. Trans.* **1998,** 3911-3917.

(26) Reynolds, J. G., The Apparent Solubility of Aluminum (III) in Hanford High-Level Waste. *J. Environ. Sci. Heal. A* **2012,** *47*, 2213-2218.

(27) Graham, T. R.; Dembowski, M.; Martinez-Baez, E.; Zhang, X.; Jaegers, N. R.; Hu, J. Z.; Gruszkiewicz, M. S.; Wang, H. W.; Stack, A. G.; Bowden, M. E.; Delegard, C. H.; Schenter, G. K.; Clark, A. E.; Clark, S. B.; Felmy, A. R.; Rosso, K. M.; Pearce, C. I., In Situ Al-27 NMR Spectroscopy of Aluminate in Sodium Hydroxide Solutions above and below Saturation with Respect to Gibbsite. *Inorg. Chem.* **2018,** *57*, 11864-11873.

(28) Du, C. H.; Zheng, S.; Zhang, Y., Phase Equilibria in the K_2O-Al_2O_3-H_2O System at 40 Degrees C. *Fluid Phase Equilibr.* **2005,** *238*, 239-241.

(29) Swaddle, T. W.; Rosenqvist, J.; Yu, P.; Bylaska, E.; Phillips, B. L.; Casey, W. H., Kinetic Evidence for Five-Coordination in $AlOH_{(aq)}^{2+}$ Ion. *Science* **2005,** *308*, 1450-1453.

(30) Graham, T. R.; Han, K. S.; Dembowski, M.; Krzysko, A. J.; Zhang, X.; Hu, J. Z.; Clark, S. B.; Clark, A. E.; Schenter, G. K.; Pearce, C. I.; Rosso, K. M., Al-27 Pulsed Field Gradient, Diffusion-NMR Spectroscopy of Solvation Dynamics and Ion Pairing in Alkaline Aluminate Solutions. *J. Phys. Chem. B* **2018,** *122*, 10907-10912.

(31) Haouas, M.; Taulelle, F.; Martineau, C., Recent Advances in Application of Al-27 NMR Spectroscopy to Materials Science. *Prog. Nucl. Mag. Res. Sp.* **2016,** *94-95*, 11-36.

(32) Swaddle, T. W.; Salerno, J.; Tregloan, P. A., Aqueous Aluminates, Silicates, and Aluminosilicates. *Chem. Soc. Rev.* **1994**, *23*, 319-325

(33) Maki, H.; Sakata, G.; Mizuhata, M., Quantitative NMR of Quadrupolar Nucleus as a Novel Analytical Method: Hydrolysis Behaviour Analysis of Aluminum Ion. *Analyst* **2017,** *142*, 1790-1799.

(34) Pilgrim, C. D.; Callahan, J. R.; Colla, C. A.; Ohlin, C. A.; Mason, H. E.; Casey, W. H., Al-27 MQMAS of the delta-Al-13-Keggin. *Dalton Trans.* **2017,** *46*, 2249-2254.

(35) Phillips, B. L.; Ohlin, C. A.; Vaughn, J.; Woerner, W.; Smart, S.; Subramanyam, R.; Pang, L., Solid-State Al-27 NMR Spectroscopy of the gamma-Al-13 Keggin Containing Al Coordinated by a Terminal Hydroxyl Ligand. *Inorg. Chem.* **2016,** *55*, 12270-12280.

(36) Oliveri, A. F.; Colla, C. A.; Perkins, C. K.; Akhavantabib, N.; Callahan, J. R.; Pilgrim, C. D.; Smart, S. E.; Cheong, P. H. Y.; Pan, L.; Casey, W. H., Isomerization of Keggin Al-13 Ions Followed by Diffusion Rates. *Chem.: Eur. J.* **2016,** *22*, 18682-18685.

(37) Holzinger, J.; Beato, P.; Lundegaard, L. F.; Skibsted, J., Distribution of Aluminum over the Tetrahedral Sites in ZSM-5 Zeolites and Their Evolution after Steam Treatment. *J. Phys. Chem. C* **2018,** *122*, 15595-15613.

(38) Vjunov, A.; Fulton, J. L.; Huthwelker, T.; Pin, S.; Mei, D. H.; Schenter, G. K.; Govind, N.; Camaioni, D. M.; Hu, J. Z.; Lercher, J. A., Quantitatively Probing the Al Distribution in Zeolites. *J. Am. Chem. Soc.* **2014,** *136*, 8296-8306.

(39) Dembowski, M.; Prange, M. P.; Pouvreau, M.; Graham, T. R.; Bowden, M. E.; N'Diaye, A. T.; Schenter, G. K.; Clark, S. B.; Clark, A. E.; Rosso, K. M.; Pearce, C. I., Inference of Principal Species in Caustic Aluminate Solutions Through Solid-State Spectroscopic Characterization. *Dalton Trans.* **2020**, *49*, 5869-5880.

(40) Kwak, J. H.; Hu, J.; Donghai, M.; Yi, C.; Kim, D. H.; Peden, C. H. F.; Allard, L. F.; Szanyi, J. Coordinatively Unsaturated Al^{3+} Centers as Binding Sites for Active Catalyst Phases of Platinum on γ-Al_2O_3. *Science* **2009**, *325*, 1670-1673

(41) Akitt, J. W.; Gessner W. Aluminum-27 Nuclear Magnetic Resonance Investigations of Highly Alkaline Aluminate Solutions. *Dalton Trans.* **1984**, *2*, 147-148

(42) Sweegers, C.; de Coninck, H. C.; Meekes, H.; van Enckevort, W. J. P.; Hiralal, I. D. K.; Rijkeboer, A., Morphology, Evolution and other Characteristics of Gibbsite Crystals Grown from Pure and Impure Aqueous Sodium Aluminate Solutions. *J. Cryst. Growth.* **2001,** *233*, 567-582.

(43) Misra, C.; White, E. T., Crystallisation of Bayer Aluminium Trihydroxide. *J. Cryst. Growth.* **1971,** *8*, 172-178.

(44) Brown, N., Secondary Nucleation of Aluminum Trihydroxide in Seeded Caustic Aluminate Solutions. *J. Cryst. Growth.* **1972,** *16*, 163-169.

(45) Hind, A. R.; Bhargava, S. K.; Grocott, S. C., The Surface Chemistry of Bayer Process Solids: A Review. *Colloid. Surface A* **1999,** *146*, 359-374.

(46) Dembowski, M.; Snyder, M. M.; Delegard, C. H.; Reynolds, J. G.; Graham, T. R.; Wang, H.-W.; Leavy, I. I.; Baum, S. R.; Qafoku, O.; Fountain, M. S.; Rosso, K. M.; Clark, S. B.; Pearce, C. I., Ion–Ion Interactions Enhance Aluminum Solubility in Alkaline Suspensions of Nano-Gibbsite (α-$Al(OH)_3$) with Sodium Nitrite/Nitrate. *Phys. Chem. Chem. Phys.* **2020**.

(47) Nikolic, I.; Blecic, D.; Blagojevic, N.; Radmilovic, V.; Kovacevic, K., Influence of Oxalic Acid on the Kinetics of $Al(OH)_3$ Growth from Caustic Soda Solutions. *Hydrometallurgy* **2004,** *74*, 1-9.

(48) Li, J.; Addai-Mensah, J.; Thilagam, A.; Gerson, A. R., Growth Mechanism and Kinetics of Gibbsite Crystallization: Experimental and Quantum Chemistry Study. *Cryst. Growth Des.* **2012,** *12*, 3096-3103

Influence of Soluble Oligomeric Aluminum on Precipitation in the Al-KOH-H_2O System

Mateusz Dembowski[†], Trenton R Graham[†], Jacob G. Reynolds[‡], Sue B. Clark[†], Kevin M. Rosso[†], and Carolyn I. Pearce[†]

[†]Pacific Northwest National Laboratory, Richland, Washington 99352, USA

[‡]Washington River Protection Solutions, LLC, Richland, Washington 93352, USA

TOC